Cage Effect in Supercritical Fluids and Compressed Gases in the Photolysis of an Asymmetrically Substituted Diazene

Pablo A. Hoijemberg,[†] Jochen Zerbs,[‡,⊥] M. Laura Japas,[§] Carlos A. Chesta,[||] Jörg Schroeder,[‡] and Pedro F. Aramendía*[,†]

INQUIMAE and Departamento de Química Inorgánica, Analítica y Química Física, Facultad de Ciencias Exactas y Naturales, Universidad de Buenos Aires, Pabellón 2, Ciudad Universitaria, 1428 Buenos Aires, Argentina, Institut für Physikalische Chemie, Georg-August Universität, Göttingen, Germany, UAQ, CNEA and UNSAM, Argentina, and Departamento de Química Facultad de Ciencias Exactas, Fisicoquímicas y Naturales, Universidad Nacional de Río Cuarto, 5800-Río Cuarto, Argentina

Received: December 24, 2008; Revised Manuscript Received: March 20, 2009

We studied the photolysis of (1-biphenyl-4-yl-1-methyl-ethyl)-*tert*-butyl diazene in supercritical CO_2 and Xe, as well as in compressed Kr. The compound has good solubility in the mentioned fluids, allowing the photolysis measurements to be performed in CO_2 at 1.4 K above T_c and at pressures as low as 70 bar. We monitored relative cage effect after nanosecond laser pulses by measuring the absorbance at 320 nm ($\Delta A_{t\rightarrow 0}$) corresponding to the total amount of out-of-cage 1-biphenyl-4-yl-1-methyl-ethyl radical (BME•) produced after nitrogen loss of the diazene. In supercritical CO_2 and Xe, isothermal values of $\Delta A_{t\rightarrow 0}$ showed an increase−decrease behavior with increasing pressure at constant temperature, a typical feature of the transition from the solvent energy transfer to the friction controlled regimes. The comparison of the behavior of $\Delta A_{t\rightarrow 0}$ in CO_2 at reduced temperatures between 1.004 and 1.027, in Xe, and in Kr points to an absence of enhanced cage effect near the critical point. Compatibility with spectroscopic data is analyzed.

1. Introduction

Supercritical fluids (SCFs) have been promoted as reaction media to replace conventional solvents in several technological processes from extraction of natural products[1] to polymer processing.[2] The main feature that makes SCFs interesting as solvents is their high compressibility: all equilibrium and transport properties that scale with the density (such as solvation power, dielectric constant, viscosity, etc.) can be tuned near the critical point by modest changes in pressure, temperature, or both.[3] Among SCFs, carbon dioxide is most frequently used because its critical point, at $T_c = 304.1$ K and $\rho_c = 73.8$ bar, is easily accessible. Moreover, CO_2 is nonflammable and nontoxic, and thus expensive steps such as solvent removal and disposal can be avoided. In addition, CO_2 is inert against reaction with free radicals, and it has already been used as solvent to perform radical polymerizations.[4−6]

For the fate of reactions in solution, the solvation of participating species is of enormous importance because it can modify reaction rates by changing activation barriers, energy transfer processes, and encounter probabilities. Despite the numerous studies performed during the last several decades, a full understanding of solvation equilibrium and dynamics in SCF has not yet been achieved. Attractive solvent−solute interactions coupled to the high compressibility of a SCF near its critical point cause a local enhancement of solvent density around low-volatile solutes, a phenomenon usually known as critical clustering. The magnitude of this enhancement can be estimated by spectroscopic data: at temperatures $T < 1.1T_c$ and densities around two-thirds of the critical value, the local solvent density around an "attractive" solute is typically 2 to 3 times larger than that of the bulk fluid.[7−10] However, the integrity of this solvation shell, that is, its strength and persistence against disruption, has not been satisfactorily characterized. In particular, several experiments indicate that because of critical clustering, products formed in the critical vicinity display a feature that is distinctive of condensed matter: a cage effect due to the enhanced local density.

In the pursuit of understanding the dynamics of reactions and the cage effect, numerous researchers have centered their attention on simple reactions, such as photocleavage and combination of free radicals.[11,12] Photolytically generated radical pairs are particularly appropriate for probing the cage effect, provided that the radicals are produced in a time that is smaller than the characteristic time of disruption of the solvation cage and react in a time comparable to the lifetime of the solvation cage. Some examples are the Norrish type I photodissociation of carbonyl compounds by cleavage of the α carbonyl bond,[13] the photo-Fries reaction of esters,[14] and the photolysis of diazenes.[15] In general, the formed radicals can combine inside the solvent cage where they were formed or diffuse away from each other and react with another diffusive radical or, eventually, with the solvent (or with a third partner, normally by H abstraction). The ratio of in-cage and out-of-cage reaction products depends on the stability of the radicals formed and on the stiffness of the solvent cage. For asymmetrically substituted ketones RCOR′ or diazenes R−N═N−R′, the analysis is frequently based on product distribution. If the radicals only combine and do not disproportionate, then R−R′ is the sole product if only reaction inside the cage occurs, whereas a 1:2:1 mol ratio of R−R/R−R′/R′−R′ is found when diffusive-pair

* Corresponding author. Tel: 54 11 4576 3378 ext. 222. Fax: 54 11 4576 3341. E-mail: pedro@qi.fcen.uba.ar.
[†] Universidad de Buenos Aires.
[‡] Georg-August Universität.
[§] UAQ, CNEA and UNSAM.
[||] Universidad Nacional de Río Cuarto.
[⊥] Present address: Institut für Verbrennungstechnik, Deutsche Gesellschaft für Luft- and Raumfahrt, Stuttgart, Germany.

10.1021/jp811390m CCC: $40.75
Published on Web 04/13/2009

radicals combine in a completely random way.[12] As an example, the photolysis of dibenzylketones asymmetrically substituted in the two rings gives nonstatistical product distribution in highly confined systems, such as zeolites, micelles, microemulsions, and polymeric matrices.[12,16−18] The product analysis becomes more complicated when disproportionation reactions play an important role.

In their photolysis study of asymmetrically substituted dibenzylketones in supercritical CO_2, Johnston and Fox[19] only found out-of-cage (escape) products. These authors interpreted this result as an indication of the weakness of the cage near the critical point. Nonetheless, the selected system was far from being ideal. The cleavage products of dibenzylketones arise from the triplet state, and CO loss from the primary benzyl-acyl radical takes place with a lifetime greater than 100 ns.[20] This creates long-lived radicals and a great amount of energy to be dissipated as heat (the difference between the absorbed energy and the energy of the stable radicals). These two effects conspire against the observation of combination products inside the cage, especially in SCF. Proof of this is that in normal liquids, the products of photolysis of asymmetrically substituted dibenzylketones also show a statistical distribution.[12]

Reactions that proceed through the singlet state, such as the photo-Fries reaction, overcome these two inconveniences. In the study of the photo-Fries reaction of naphthyl acetate in supercritical CO_2, Weedon and collaborators[21] found a rise of almost a factor of three in the yield of combination (in-cage) products in a narrow range of 20 bar near the critical pressure. They interpreted this result in terms of the formation of long-lived solvent−solute clusters effectively changing the course of the reaction. However, their results are controversial because in-cage product yields were larger under near-critical conditions than in dense liquid CO_2. As the authors point out, it is counterintuitive to conceive that the efficiency of the solvation shell to restrict molecular motions in the compressed fluid at 35 °C and 350 bar ($\rho \approx 22$ mol dm^{-3}, ca. $2\rho_c$) can be insignificant compared with that of fluid at the same temperature and 76 bar (bulk density of 7 mol dm^{-3}, ca. 0.7 ρ_c), even considering for the latter case a factor of three in the augmentation of solvent density around the solute.

Recently, Pacut and Tanko[22] studied the cage effect in SCF by the photolysis of dicumylketone in supercritical CO_2. They found that the ratio between escape and in-cage products reached a maximum at pressures close to the critical pressure. As the density increases, the decrease in escape products is easily understood in terms of the rising viscosity; however, the behavior in the low density region in terms of critical clustering is again counterintuitive: escape product yields were lower at $\rho \approx 0.4\ \rho_c$ than in the dense fluid. Actually, the increase−decrease behavior of some rate constants as a function of medium density does not differ from what was previously observed by other authors in combination and isomerization reactions under compressed gases, namely, the transition between the energy transfer regime to that governed by diffusion and solvent viscosity.[23,24] The mentioned work was performed at 323 K, probably to avoid limitations in concentration of the probe due to its low solubility. Therefore, the lack of evidence of an enhanced cage effect can be attributed to experimental conditions that are too remote from the critical point to show typical effects of this phenomenon. However, in the free radical chlorination of alkanes, there was no indication of an enhanced cage effect on the products of the reaction between alkyl radicals and chlorine in the vicinity of the critical point in SC−CO_2.[25]

An adequate probe for monitoring the cage effect of radical reactions in SCF should meet several requirements, some of which can be deduced from the previous discussion. It should rapidly, irreversibly, and efficiently produce a pair of geminate radicals by irradiation. We chose a diazene because they do not revert to the parent compound after dissociation and loss of nitrogen.[15] However, because diazenes are generally thermally labile; its thermal stability in the working temperature range had to be assured. To favor dissociation and hinder isomerization, the other major deactivation pathway for excited diazenes, bulky groups next to the N atoms need to be added. The probe should also be soluble enough under compressed gases and SCF, near and preferably below ρ_c, to produce a concentration of radicals after photolysis that is large enough to be monitored. High absorption coefficients of the probe allow small amounts of it to dissolve while attaining absorbance values adequate for photochemical experiments. Therefore, adding an antenna group to transfer the absorbed energy to the reactive group is also valuable.

To attend to all of these requirements, we synthesized a diazene with two methyl groups in the C atoms next to the N atoms and biphenyl group as a UV light antenna.[26] In this work, we examine the photolysis of (1-biphenyl-4-yl-1-methyl-ethyl)-*tert*-butyl-diazene, aiming to its use as a cage effect probe in SCF. The diazene compound is a relatively volatile solid that is thermally stable up to 343 K and dissolves in SCF at densities below the critical value, allowing photoreaction experiments to be performed less than 2 K above T_c. The diazene has a highly absorbing π,π^* band and a weak n,π^* band with maximum absorption at 254 and at 365 nm, respectively.

Picosecond and microsecond flash photolysis experiments were performed in a solution of common liquids such as cyclohexane and *n*-hexane to understand the photochemical mechanism of radical production.[27] Upon excitation in the π,π^* band, the biphenyl-centered excited state is produced, which has a lifetime of 3.5 ps. It decays to the excited singlet n,π^* state, which is dissociative. A small amount of the biphenyl-centered triplet is also produced. Irradiation on the n,π^* band shows the build up of the typical benzyl-type radical absorption around 320 nm with a risetime of 0.7 ps. The favorable structural and photochemical characteristics of the diazene allowed the cage effect study in SCF to be performed by following the amount of the 1-biphenyl-4-yl-1-methyl-ethyl (BME•) radical formed after nanosecond laser pulse excitation. Our results, obtained in different fluids such as supercritical CO_2, Xe, and Kr, suggest the absence of enhanced cage effect under near-critical conditions.

2. Experimental Section

Complete experimental information is detailed in the Supporting Information.

Materials. The detailed synthesis of the diazene used in this work is described elsewhere.[26]

We checked the O_2 level of the CO_2 (Praxair, 4.8) by measuring the triplet decay lifetime of fluorenone (Merck, for synthesis) dissolved in CO_2 under conditions similar to those of the photolysis experiments but irradiating at 354 nm. Observed lifetimes were larger than 25 μs.

The following chemicals were used without further purification: Xe (AGA, Research Quality, 99.995%, $O_2 < 3$ ppm), Kr (Messer Griesheim, 4.7, $O_2 < 0.5$ ppm), cyclohexane (Sintorgan, HPLC grade), and naphthalene (Merck, for synthesis).

Absorption and Emission Spectra. Absorption spectra were determined using either a Hewlett-Packard 6453E diode array,

a Shimadzu 160A apparatus, or a Shimadzu PC3100 spectrophotometer (liquid solutions at atmospheric pressure) or on a Shimadzu UV3101PC (high-pressure cell). Fluorescence spectra were recorded using a PTI-Quantamaster spectrofluorometer.

Sample Preparation. For the high-pressure measurements, a homemade stainless steel cell was used, as in previous work.[28] It comprises three sapphire windows (10 mm diameter and 5 mm width), gas inlet and outlet, and an inlet to place a calibrated thermistor for temperature monitoring. We prepared solutions in supercritical CO_2, Xe, and Kr by adding proper amounts of solution of the diazene in cyclohexane (Sintorgan, HPLC grade) to obtain a final absorbance of around 0.5 and 0.8 along the ca. 10 mm photolysis light path. Solvent was then evaporated, and the cell was carefully purged to remove the oxygen. The SCF was added by either a manual pressure generator or an automatic high-pressure syringe (ISCO DM-100). For isothermal runs, measurements were performed by successive injections of gas at constant temperature. For isochoric runs in CO_2 (at constant SCF molar volume), the amount of SCF was kept constant, and the temperature was increased and decreased.

It was mandatory to perform all measurements without crossing a phase boundary, that is, to make sure that all solutions of the diazene in the SCF were subsaturated. Therefore, in separate experiments, the solubility of the diazene was determined as a function of pressure for each investigated gas. Data points where dissolution of the sample was not complete were not taken into account.

Laser Flash Photolysis. ***Microsecond Regime Measurements.*** Transient absorption spectra of diazene samples at high pressure were determined by excitation with a Spectron SL400 Nd:YAG laser generating 266 nm pulses (ca. 10 ns pulse width).[29] We used solutions of naphthalene in cyclohexane to optimize transient signals, both spatially and instrumentally, by analyzing the amplitude of triplet production at 420 nm. Fixed wavelength traces were used to reconstruct time-resolved difference spectra.

Picosecond Regime Measurements. Details of the experimental setup with UV−visible detection have been described elsewhere.[30] A commercial 1 kHz Ti/sapphire regenerative amplifier (Clark-MXR CPA2001) was used as the light source, delivering pulses of 150 fs duration and an energy of 0.9 mJ centered at a wavelength of 773 nm. Probe pulses were generated in a TOPAS (Light Conversion) covering the wavelength range from 285 to 750 nm. We obtained pump pulses of 387 nm by generating the harmonic of the laser fundamental. The experiments were carried out under magic angle polarization.

High-pressure time-resolved measurements in the picosecond regime were performed in a different high-pressure cell. The basic design of the stainless steel high-pressure sample cell was developed by Prof. O. Kajimoto's group at Kyoto University.[31] It contains a small sample reservoir and a magnetic stirrer, and its effective optical length between sapphire windows of 2 mm thickness is 2.5 mm.

For transient absorption measurements, the sample reservoir was filled with a defined amount of solid diazene before the cell was pressurized with CO_2. The pump and probe wavelengths were set to 387 and 330 nm, respectively.

3. Results

The solubility of the diazene in SCF was determined along isotherms. Figure 1 shows the results for CO_2 and Kr at 308 K and for Xe at 313 K as a function of fluid density; the latter was calculated from measured pressure and temperature using a proper equation of state, EoS.[32] As has been found previously,[33] the logarithm of the solubility varies almost linearly with the density. The slope of this representation for CO_2 was found to be almost independent of temperature up to 323 K. Therefore, the isotherms corresponding to higher temperatures are parallel curves shifted toward higher solubility.

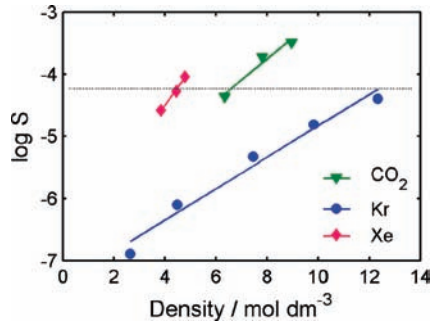

Figure 1. Logarithm of diazene solubility (S in units of mol dm^{-3}) as a function of solvent bulk density. The horizontal dotted line represents the logarithm of the minimum concentration required for flash photolysis experiments. Solubility was measured at 308 K for CO_2 and Kr and at 313 K for Xe. Green triangles represent carbon dioxide, blue circles represent krypton, and magenta diamonds represent xenon data points.

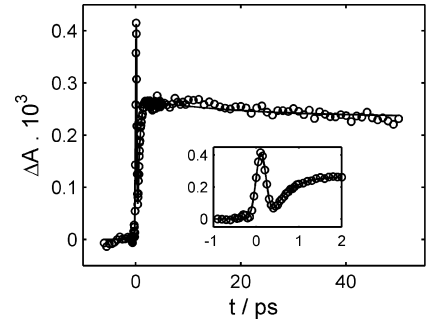

Figure 2. Transient difference absorption signal after femtosecond photolysis of the diazene in supercritical carbon dioxide at 155 bar and 308 K with pump at 387 nm and monitored at 330 nm: ○, averages from six traces; —, fit function comprising a Gaussian peak for excitation, an exponential rise, and a biexponential decay. The inset shows the rise in detail, which occurs in about 0.7 ps.

The build up of the BME• radical in supercritical CO_2 is shown in Figure 2 after femtosecond laser excitation at 387 nm. Considering the low ground-state absorption in the n,π^* band ($\lambda_{max} = 365$ nm; $\varepsilon = 75 \pm 10$ M^{-1} cm^{-1}), experiments in this region can only be performed at relatively high diazene concentrations, which can hardly be achieved at $\rho < 2\rho_c$. Irradiation of the diazene in the band at 254 nm populates the biphenyl centered $^1\pi,\pi^*$ excited state, which decays in ca. 3.5 ps to the dissociative ^{1}n,π^*. The intense absorption bands of the $^1\pi,\pi^*$ obscure the build up of the BME• radical.[27,34] Therefore, the build up of the radical cannot be monitored in this way in the low-pressure range. Increasing the CO_2 pressure above 155 bar does not show any change in the BME• radical time trace. The similar lifetimes measured for BME• radical build up in cyclohexane[27] and condensed CO_2 indicates that at 155 bar, the condensed liquid kinetic behavior is already reached for diazene dissociation.

Nanosecond flash photolysis shows an instantaneous increase (on this time scale) in out-of-cage BME• radical absorption. In the microsecond regime, we can observe only the out-of-cage decay reactions of the BME• radical. Figure 1 in the Supporting Information shows decays of the BME• concentration in Xe at 313 K and different pressures. A time-zero extrapolation of the nanosecond flash-photolysis measurements provides a way of

quantifying how many of these radicals escape their original cage. More precisely, the absorbance change at time zero ($\Delta A_{t\to 0}$) is given by eq 1

$$\Delta A_{t\to 0} \propto \phi_{\mathrm{BME}\cdot,\mathrm{free}} = \phi_{\mathrm{diss}} \frac{k_{\mathrm{esc}}}{k_{\mathrm{esc}} + k_{\mathrm{c}} + k_{\mathrm{d}}} \qquad (1)$$

where ϕ_{diss} is the quantum yield of radical production by bond photocleavage. It is multiplied by the escape probability of the geminate radicals. As expressed by eq 1, this latter probability is the ratio between the rate constant for cage escape, k_{esc}, and the sum of this constant and the rate constants for reaction of the geminate radicals BME· and *t*-Bu· inside the cage, k_{c} and k_{d}. These two account, respectively, for combination and for both types of disproportionation. The proportionality constant includes the concentration of the diazene, the absorption coefficient of the radical at the analysis wavelength, and the absorbed light dose during the pulse and instrumental factors, such as the overlap of the analysis beam path with the photolyzed volume. Because the alignment of the high-pressure cell may vary from run to run (it has to be dismounted for cleaning and reloading), the comparison of data from different runs on a unique and absolute scale is not advisible. However, throughout the same batch, all alignment-dependent factors are carefully maintained to be constant. The same applies for the concentration of the diazene, which we kept constant within a run by working under subsaturation conditions and by proceeding, along each isothermal run, only by the addition of the SCF. Therefore, to compare the results of different runs, for each of them, we normalized the data by arbitrarily assigning the value of 1 to the highest value.

Figure 2 in the Supporting Information shows the normalized absorbance difference at time zero for the diazene photolyzed in CO_2, Kr, and Xe at 313 K as a function of the pressure.

The pressure is not a relevant variable to microscopically characterize the system. Instead, a better choice is to use the inverse diffusion coefficient, D^{-1}, a variable that measures the effective collision frequency.[23] To convert pressure data to D^{-1}, a few steps are necessary. First, the pressure and temperature are used as inputs in REFPROP to obtain density and viscosity for each solvent condition.[32] Then, a good approximation for the diffusion coefficient can be obtained from viscosity, η, and density, ρ, through eq 2, which is an empirical extension of the Stokes−Einstein relation to low fluid density[35,36]

$$\frac{k\mathrm{T}}{\eta D} \cong 3\pi\sigma\left\{1 - \exp\left(-\frac{\rho}{\rho_{\mathrm{c}}}\right)\right\} \qquad (2)$$

where k is the Boltzmann constant and σ is the Lennard-Jones diameter of the diffusing species. This last quantity was derived from the geometrical volume of BME· radical: 0.195 nm^3.[37] A spherical shape was assumed to obtain a σ value of 0.72 nm, which was used for the calculations in eq 2.

In Figure 3, the normalized absorbance differences at time zero are plotted for diazene photolyzed at 313 K in CO_2, Kr, and Xe versus D^{-1} (on the logarithmic scale). Finally, Figure 4 shows the normalized absorbance difference at time zero for the diazene photolyzed in CO_2 at 305.5, 308.0, and 313.0 K as a function of D^{-1} (on the logarithmic scale).

Two isochores were performed under CO_2 at densities around 18 and 20.5 mol dm^{-3}, changing the temperature between 305.5 and 312 K. As can be seen in Table 1, while changing the temperature about 6 K (with viscosity and diffusion coefficient varying <1%), an increase of ca. 15% on the absorbance at time zero is obtained. This increase results in an activation energy of 20 ± 10 kJ mol^{-1} for the production of BME· radicals. Even though the temperature range is small and the $\Delta A_{t\to 0}$ values have a relatively large uncertainty (ca. 10%), the results clearly show that the activation energy for the production of BME· radicals is significantly higher than the activation energy of the friction.

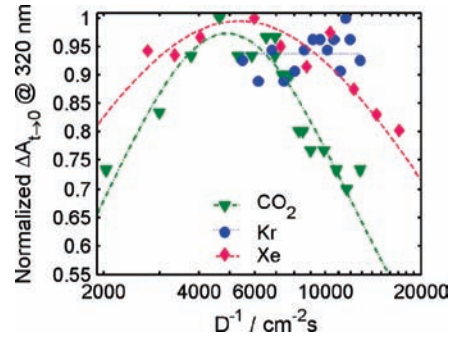

Figure 3. Time zero extrapolation (on the nanosecond scale) of the differential absorbance ($\Delta A_{t\to 0}$) after excitation of the diazene dissolved in supercritical solvent at 313 K as a function of the inverse diffusion coefficient. The highest value in each set was normalized. Pump wavelength is 266 nm, and probe wavelength is 320 nm. ▼, ●, and ♦ represent carbon dioxide, krypton, and xenon data points, respectively. Lines represent the fits to the function $\Delta A_{320\mathrm{nm}}(t = 0) \propto \phi_{\mathrm{BME}\cdot,\mathrm{free}} \propto (A\cdot D + B + C/D)^{-1}$. (See the text.) The values of the coefficients are given in Table 2. − · −, · · ·, and − − − are fit lines for carbon dioxide, krypton, and xenon data, respectively. In the case of Kr, only an average of the almost constant data is shown.

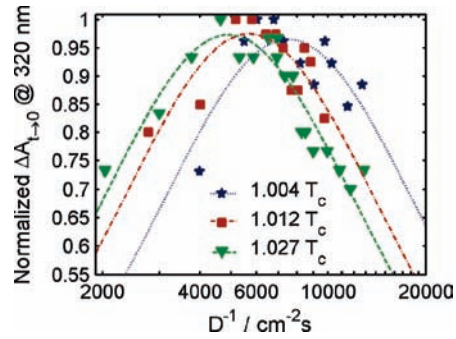

Figure 4. Time zero extrapolation (on the nanosecond scale) of the differential absorbance ($\Delta A_{t\to 0}$) after excitation of the diazene dissolved in supercritical carbon dioxide at different reduced temperatures as a function of the inverse diffusion coefficient. Normalization is done to the highest value in each set. Pump wavelength is 266 nm and probe wavelength is 320 nm. ★, ■, and ▼ are data at 1.004T_c, 1.012T_c, and 1.027T_c, respectively. Lines represent the fits to the function $\Delta A_{320\mathrm{nm}}(t = 0) \propto \phi_{\mathrm{BME}\cdot,\mathrm{free}} \propto (A\cdot D + C/D)^{-1}$. (See the text.) · · ·, − · −, and − − − are fit lines for 1.004T_c, 1.012T_c, and 1.027T_c, respectively. The values of the coefficients are given in Table 2.

TABLE 1: Formation of BME· Radicals As a Function of Temperature in Two Experiments Performed at Constant Composition

pressure (bar)	temperature (K)	density (mol dm^{-3})	ΔA_{max} (320 nm)	viscosity (10^{-2} mPa s)	D (10^3 cm^2 s^{-1})
236.6	305.4	20.6	0.013	9.26	12.8
255.8	307.5	20.6	0.014	9.33	12.8
285.6	311.5	20.6	0.019	9.34	12.6
133.9	305.6	18.4	0.0088	7.28	9.64
138.0	307.5	18.3	0.0093	7.15	9.38
148.0	312.0	17.9	0.0101	6.86	8.81

4. Discussion

Even though the main point of this work is the question of whether there is an enhanced cage effect associated with radical

TABLE 2: Values of the Fitted Parameters from Equation 5 to the Data for Xe in Figure 3 and CO_2 in Figure 4 of the Equivalent Friction at the Maximum, D^{-1}_{max}, (Equation 6) and of Its Corresponding Reduced Density $(\rho/\rho_c)_{max}$

	A (10^3 s cm^{-2})	B	C (10^{-5} cm^2 s^{-1})	D^{-1}_{max} (10^3 s cm^{-2})	$(\rho/\rho_c)_{max}$
CO_2 305.5 K	4.0 ± 0.5		6.7 ± 0.8	7.7 ± 1.0	1.56 ± 0.10
CO_2 307 K	3.0 ± 0.3		8.9 ± 0.8	5.8 ± 0.6	1.36 ± 0.07
CO_2 313 K	2.5 ± 0.2		10.5 ± 0.6	4.9 ± 0.3	1.25 ± 0.05
Xe 313 K	1.0 ± 0.6	0.6 ± 0.2	3.7 ± 1.0	5.3 ± 2.2	1.0 ± 0.2

reactions in SCFs, it is important to understand the photophysical details of production of the BME• radical and its photochemistry to support its suitability to probe this effect. First, the diazene has a biphenyl moiety with a high absorption coefficient that allows us to perform experiments at temperatures extremely near the critical point. Second, there is an efficient internal electronic energy transfer process ($^1\pi,\pi^*$ to ^{1}n,π^*), that produces the dissociative state (^{1}n,π^*). Third, a fast nitrogen loss takes place, and the produced radicals experience different types of reaction in the cage. In particular, the competition between combination and disproportionation is important to analyze the pressure dependence of free BME• radical production. Fourth, the BME• radical has favorable spectroscopic characteristics to be easily monitored.

Excitation of the diazene at 275 nm populates the $^1\pi,\pi^*$ state, which decays in 3.5 ps, populating the dissociative ^{1}n,π^* excited state with a very high efficiency.[27] Therefore, the presence of the diazo moiety in the diazene, with its dissociative ^{1}n,π^* state acting as a funnel of the electronic energy, is responsible for the short lifetime of the diazene's biphenyl-centered $^1\pi,\pi^*$, and C−N bond dissociation is responsible for the extremely short excited-state lifetime of the diazene ^{1}n,π^*.

The photophysical and photochemical events of the diazene leading to the production of free BME• radicals in solution are summarized in Scheme 1.

The quantum yield of production of out-of-cage BME• radicals is derived according to the kinetic Scheme 1

$$\phi_{BME\bullet,free} = \frac{k_{ET}}{k_{ET}+k_{deac}}\frac{k_{diss}}{k_{diss}+k_{nr}}\frac{k_{esc}}{k_{esc}+k_{reac}} \qquad (3)$$

where k_{ET} is the rate constant for conversion of $^1\pi,\pi^*$ to ^{1}n,π^*, k_{deac} is the sum of internal conversion to the ground-state and intersystem crossing processes from the initially excited $^1\pi,\pi^*$ state, k_{diss} is the dissociation rate constant, k_{nr} is the sum of all competitive processes degrading electronic energy from the dissociative ^{1}n,π^* excited state without producing radicals, and k_{reac} is the sum of all reactive rate constants of the geminate radicals in the cage after N_2 loss.

The plots in Figures 3 and 4 for the BME• radical always show a bell-shaped behavior as a function of variables related to the density (or pressure) or related to friction (viscosity or inverse BME• radical diffusion coefficient).

The shape of the curves is a result of the medium effect in two different processes. At low pressures, the increase in collision frequency promotes the dissociation of the electronically excited diazene, which causes $\phi_{BME\bullet,free}$ to rise. At high pressure, the confinement lowers the escape probability, favoring in-cage reaction.

In what follows, we will analyze the collision dependence of all rate constants involved in eq 3 to infer the total friction dependence of free diffusing BME• radicals.

The first point is to identify the process or processes responsible for the increase in the radical yield with increasing collision frequency. We can assume that dissociation is a barrier-controlled process. The absorption of a photon of 266 nm to excite the diazene to the $^1\pi,\pi^*$ state implies an input of ca. 470 kJ mol^{-1}. However, the dissociative ^{1}n,π^* is ~330 kJ mol^{-1} above the ground state (corresponding to an absorbed photon of 365 nm). Assuming that there is a finite energy barrier on the dissociative ^{1}n,π^* state because of transfer of an electron to a C-centered σ^* orbital, this energy barrier could be on the order of 10 kJ mol^{-1}. The 140 kJ mol^{-1} energy release upon internal conversion would make such an energy barrier practically unnoticeable for an excited state living 0.7 ps. The one to four collisions during this lifetime would by far not suffice to dissipate this energy into the solvent.

Therefore, no pressure dependence can be expected on processes taking place from the ^{1}n,π^* state after excitation to the $^1\pi,\pi^*$ state.

As a consequence, we suggest that $^1\pi,\pi^*$ to ^{1}n, π^*, that is, the internal electronic energy transfer step, must be the density-dependent step and be responsible for the observed rise in the radical yield with pressure. It could be either collision-induced or caused by a relative shift of the two potential surfaces as a consequence of increasing refractive index (dispersive interactions). It might also be slightly temperature-dependent, depending on where the conical intersection between the two surfaces is located.

If k_{ET} is promoted by collisions, then $k_{ET} = a\bullet D^{-1}$. On the other side, k_{esc} is slowed down by friction, meaning that $k_{esc} = b\bullet D$. The reactive rate constant, k_{reac}, is a sum of two processes: combination (k_c) and disproportionation (k_d). Radical combination has a higher influence on friction because of its higher sterical requirements than H abstraction from an isopropyl moiety.[22] Formally, $k_{reac} = k_d + k_c = \alpha + \beta\bullet D$. Assuming that k_{deac}, is not affected by friction and that, as discussed above, no process of the ^{1}n,π^* state is affected by density, eq 3 can be written as

$$\phi_{BME\bullet,free} \propto \frac{a\cdot D^{-1}}{a\cdot D^{-1}+k_{deac}}\frac{b\cdot D}{\alpha+(b+\beta)\cdot D} = \frac{a\cdot b}{a\bullet\alpha\bullet D^{-1}+(b+\beta)\cdot k_{deac}\cdot D+[a\cdot(b+\beta)+k_{deac}\cdot\alpha]} \qquad (4)$$

Equation 4 has the functional form of a process that is promoted by collisions at low pressure, and that at high pressure is hindered by friction.[23]

The bell-shaped curves in Figures 3 and 4 correspond to the fit of experimental data to a function of the form

$$\Delta A_{320nm}(t=0) \propto \phi_{BME\bullet,free} \propto (A\cdot D + B + C/D)^{-1} \qquad (5)$$

where the adjustable constant A is responsible for the high friction behavior, C accounts for the low friction behavior, and B describes the friction-independent contribution. In CO_2, this latter term proved to be unimportant, meaning that the actual values are far from the upper friction-independent limit. Therefore, the simplified equation was used for CO_2, yielding fitting constants with higher significance. The data in Xe could be adequately fitted with only the three-parameter equation.

The fitted parameters can be used to calculate $(D^{-1})_{max}$, the inverse diffusion coefficient that corresponds to the maximum of the curves

$$(D^{-1})_{max} = \sqrt{A/C} \qquad (6)$$

where the two friction-dependent terms in eq 5 are equal. The fitted parameters of eqs 5 and the calculated values of $(D^{-1})_{max}$

SCHEME 1: Dynamics for the Asymmetrically Substituted Diazene Dissociation upon Irradiation with UV Light

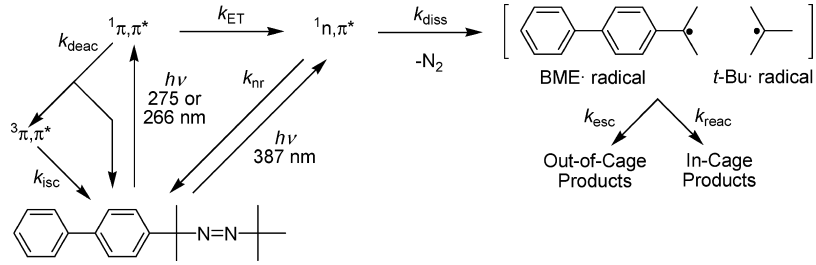

for the data of Figures 3 and 4, together with their corresponding densities, are summarized in Table 2.

As shown in Table 2, for CO_2, the maximum value of $\Delta A_{t\to 0}$ always occurs at a density higher than the critical density, ρ_c. (Because of the wideness of the Xe curve, the uncertainty of its $D^{-1}{}_{max}$ and ρ_{max} is too large to be significant.) In CO_2, upon temperature increase, the friction needed to reach the maximum free radical yield decreases (Figure 4); that is, $D^{-1}{}_{max}$ and ρ_{max} shift to lower values. This indicates an increase in the internal conversion rate constant with temperature, giving rise to an apparent activation barrier (see below), which is a well-known density of states effect.[38] This conclusion is also compatible with the increase in free BME· signal with temperature along isochores; as shown in Table 1, an increase in temperature favors the production of free diffusing BME· radicals. The temperature range is nevertheless too small to obtain useful activation parameters. The data in Table 1 are compatible with an apparent activation barrier of 20 ± 10 kJ mol^{-1} for the internal conversion, whereas those of the viscosity plays a much smaller role (ca. 1 kJ mol^{-1} for CO_2). These facts confirm that the $^1\pi,\pi^*$ to ^{1}n, π^* internal electronic energy transfer step is an activated process.

The increase in the value of the friction needed to attain the maximum in the efficiency of production of free diffusing radicals as the system approaches the critical isotherm (from higher temperatures) is contrary to what should be expected from an enhanced clustering around the probe caused by critical susceptibility. If clustering should prevent radicals from escaping the cage, then the beginning of the decrease in free diffusing radical production should take place at lower bulk friction than that corresponding to the critical density.

Moreover, at ρ_c, the production of free diffusing BME· radicals is still promoted by collisions (Figure 4 and Table 2), contrary to what would be expected from an enhanced cage effect. Furthermore, no anomalous behavior is detected around ρ_c in any of the isotherms and no difference between the behavior in Xe and that in CO_2 is observed. These facts point to the absence of an enhanced cage effect near the critical point. We will further reinforce these arguments.

The enhanced cage effect is associated with a collision frequency increase around the reactants because of a local density augmentation around them. In SCF, density inhomogeneities are allowed by the high compressibility of the fluid. The size of the inhomogeneous domains, called the correlation length, ξ, diverges at the critical point because ξ^2 is proportional to the compressibility. At $\rho = \rho_c$, the dependence of ξ with the distance to the critical point, measured by the value of $\tau = (T - T_c)/T_c$, is given by $\xi = \xi_0\tau^{-\nu}$, where $\nu = 0.63$ is a universal critical exponent and ξ_0 is a system-dependent amplitude.[39] For CO_2, $\xi_0 = 0.149$ nm;[39] the correlation lengths, ξ, at the critical density are 4.8 nm ($10\sigma_{CO_2}$) at 305.5 K, 2.4 nm ($5\sigma_{CO_2}$) at 307 K, and 1.45 nm ($3\sigma_{CO_2}$) at 313 K, where σ_{CO_2} represents the Lennard-Jones diameter of the molecule. In other words, a change in temperature from 305.5 to 313 K produces a decrease in the correlation length by a factor of three, whereas the number of solvent molecules implicated in the correlation volume drops by a factor of 30. If critical clustering was of a great importance in the dissociation of the diazene, an increase in reduced temperature by a factor of seven, from 305.5 to 313 K, should drastically reduce its participation. There is no evidence of this in the experiences in CO_2, rather the three isotherms seem very much alike.

The relative BME· radical production yield in CO_2, Xe, and Kr as a function of D^{-1} shows different trends at 313 K. The plateau is greatest in Kr, and sharpest in CO_2, following the decrease in reduced temperature. The decay of the yield in the high-pressure range is steeper for CO_2. The behavior of the radical yield in Kr can be well interpreted as being almost constant in the pressure range studied. Though the lower limit of this pressure range is established by the solubility of the diazene (which imposes a limit on the absorbance needed for the experiment), the overall pressure range in Kr (240 to 590 bar) is not smaller than that for the other gases (70 to 400 bar for Xe and 67 to 305 bar for CO_2). The pressure dependence of the diffusion coefficient is milder for Kr than for the other gases in their investigated density ranges because Kr is at a much higher reduced temperature at 313 K. The rise in the yield is practically equal for Xe and CO_2, implying that the collision frequency equally influences the internal conversion step in both media. At 313 K, the viscous effect causing a decrease in the radical yield in CO_2 appears at a slightly lower bulk friction than that in Xe and is not observed in Kr. This can be related to the decrease in the solvent−solvent molecular interactions following this sequence.

Clustering of solvent around a probe in the vicinity of the solvent critical point is a well-documented effect in spectroscopic studies. This effect, though thoroughly looked for, has not been unequivocally proven up to now in chemical processes (isomerization, dissociation, or combination reactions). On the contrary, most of the results show the absence of such an effect. In our opinion, the solute−solvent interactions responsible for the clustering are so weak that the energy released during the reaction or in preceding steps is large enough to disrupt the cluster. Therefore, the two observations are not incompatible.

Acknowledgment. C.A.C. and P.F.A. are research staff from CONICET (Consejo Nacional de Investigaciones Científicas y Técnicas, Argentina). P.A.H. is a Ph.D. fellow from CONICET and thanks DAAD (Deutscher Akademischer Austauschdienst) for a research grant. This work was performed under financial support from ANPCyT (PICT02 06-10621 and 06-33973) and UBA (X086).

Supporting Information Available: Complete experimental information, differential absorbance in the first 16 μs after excitation of the diazene in supercritical Xe at 313 K as a

function of pressure, and time zero extrapolation (on the nanosecond scale) of the differential absorbance ($\Delta A_{t\rightarrow 0}$) after excitation of the diazene dissolved in supercritical solvent at 313 K as a function of pressure. This material is available free of charge via the Internet at http://pubs.acs.org.

References and Notes

(1) Kaiser, C. S.; Römpp, H.; Schmidt, P. C. *Pharmazie* **2001**, *56*, 907–926.

(2) DeSimone, J. M.; Maury, E. E.; Menceloglu, Y. Z.; McClain, J. B.; Romack, T. J.; Combes, J. R. *Science* **1994**, *265*, 356–359.

(3) Fernández-Prini, R.; Japas, M. L. *Chem. Soc. Rev.* **1994**, *23*, 155–163.

(4) Ahmed, T. S.; DeSimone, J. M.; Roberts, G. W. *Macromolecules* **2007**, *40*, 9322–9331.

(5) Cao, L. Q.; Chen, L. P.; Jiao, J. Q.; Zhang, S. Y.; Gao, W. *Science* **2007**, *285*, 1229–1236.

(6) Bunyard, W. C.; Kadla, J. F.; DeYoung, J.; DeSimone, J. M. *J. Am. Chem. Soc.* **2001**, *123*, 7199−7206; **2003**, *125*, 11772 (addition/correction).

(7) Song, W.; Biswas, R.; Maroncelli, M. *J. Phys. Chem. A* **2000**, *104*, 6924–6939.

(8) Okamoto, M.; Nagashima, H.; Tanaka, F. *Phys. Chem. Chem. Phys.* **2002**, *4*, 5627–5633.

(9) Aizawa, T.; Kanakubo, M.; Hiejima, Y.; Ikushima, Y.; Smith, R. L. *J. Phys. Chem. A* **2005**, *109*, 7353–7358.

(10) Cabaço, M. I.; Longelin, S.; Danten, Y.; Besnard, M. *J. Phys. Chem. A* **2007**, *111*, 12966–12971.

(11) Brennecke, J. F.; Chateauneuf, J. E. *Chem. Rev.* **1999**, *99*, 433–452.

(12) Turro, N. J.; García-Garibay, M. A. In *Photochemistry in Organized and Constrained Media*; Ramamurthy, V., Ed.; VCH: New York, 1991; pp 1−38.

(13) Turro, N. J. *Modern Molecular Photochemistry*; University Science Books: Mill Valley, CA, 1991; pp 528−534.

(14) Stumpe, J.; Selbmann, Ch.; Kreisig, D. *J. Photochem. Photobiol., A* **1991**, *58*, 15–30.

(15) Engel, P. S. *Chem. Rev.* **1980**, *80*, 99–150.

(16) Nageshwer Rao, B.; Syamala, M. S.; Turro, N. J.; Ramamurthy, V. *J. Org. Chem.* **1987**, *52*, 5517–5521.

(17) Hrovat, D. A.; Liu, J. H.; Turro, N. J.; Weiss, R. G. *J. Am. Chem. Soc.* **1984**, *106*, 7033–7037.

(18) Chesta, C. A.; Mohanty, J.; Nau, W. M.; Bhattacharjee, U.; Weiss, R. G. *J. Am. Chem. Soc.* **2007**, *129*, 5012–5022.

(19) O'Shea, K. E.; Combes, J. R.; Fox, M. A.; Johnston, J. P. *Photochem. Photobiol.* **1991**, *54*, 571–576.

(20) Gould, I. R.; Baretz, B. H.; Turro, N. J. *J. Phys. Chem.* **1987**, *91*, 925–929.

(21) Andrew, D.; Des Islet, B. T.; Margaritis, A.; Weedon, A. C. *J. Am. Chem. Soc.* **1995**, *117*, 6132–6133.

(22) Tanko, J. M.; Pacut, R. *J. Am. Chem. Soc.* **2001**, *123*, 5703–5709.

(23) Troe, J. *J. Phys. Chem.* **1986**, *90*, 357–365.

(24) Lee, M.; Holtom, G. R.; Hochstrasser, R. M. *Chem. Phys. Lett.* **1985**, *118*, 359–363.

(25) Fletcher, B.; Suleman, N. K.; Tanko, J. M. *J. Am. Chem. Soc.* **1998**, *120*, 11839–1844.

(26) Hoijemberg, P. A.; Karlen, S.; Sanramé, C. N.; Aramendía, P. F.; García-Garibay. M. A. *Photochem. Photobiol. Sci.*, published online March 30 2009, http://dx.doi.org/10.1039/b902272d.

(27) Hoijemberg, P. A.; Zerbs, J.; Reichardt, C.; Schwarzer, D.; Chesta, C. A.; Schroeder, J. Aramendía, P. F. Photophysics and photochemistry of an asymmetrically substituted diazene: an adequate cage effect probe. *J. Phys. Chem. A*, accepted for publication.

(28) Wetzler, D. E.; Fernández-Prini, R.; Aramendía, P. F. *Chem. Phys.* **2004**, *305*, 27–36.

(29) Rivarola, C. R.; Bertolotti, S. G.; Previtali, C. M. *J. Polym. Sci., Part A: Polym. Chem. Ed.* **2001**, *39*, 4265–4273.

(30) Grimm, C.; Kling, M.; Schroeder, J.; Troe, J.; Zerbs, J. *Israel J. Chem.* **2003**, *43*, 305–317.

(31) Grimm, C.; Kandratsenka, A.; Wagener, P.; Zerbs, J.; Schroeder, J. *J. Phys. Chem. A* **2006**, *110*, 3320–3329.

(32) Lemmon, E. W.; Huber, M. L.; McLinden, M. O. Reference Fluid Thermodynamic and Transport Properties (REFPROP), NIST Standard Reference Database 23, version 8.0; Physical and Chemical Properties Division, NIST: Boulder, CO, 2007. The REFPROP program "is based on the most accurate pure fluid and mixture models currently available. It implements three models for the thermodynamic properties of pure fluids: equations of state explicit in Helmholtz energy, the modified Benedict−Webb−Rubin equation of state, and an extended corresponding states (ECS) model. Viscosity and thermal conductivity are modeled with either fluid-specific correlations, an ECS method, or in some cases the friction theory method".

(33) Sciaini, G.; Marceca, E.; Fernández-Prini, R. *J. Supercrit. Fluid.* **2005**, *35*, 106–110.

(34) Kato, C.; Hamaguchi, H.-O.; Tasumi, M. *Chem. Phys. Lett.* **1985**, *120*, 183–187.

(35) Otto, B.; Schroeder, J.; Troe, J. *J. Chem. Phys.* **1984**, *81*, 202–213.

(36) Hippler, H.; Schubert, V.; Troe, J. *Ber. Bunsen-Ges. Phys. Chem.* **1985**, *89*, 760–763.

(37) Edward, J. T. *J. Chem. Educ.* **1970**, *47*, 261–270.

(38) Klessinger, M.; Michl, J. *Excited States and Photochemistry of Organic Molecules*; VCH: New York, 1995.

(39) Sengers, J. V.; Levelt Sengers, J. M. H. *Annu. Rev. Phys. Chem.* **1986**, *37*, 189–222.

JP811390M